Research Article

Qiuyun Zhang*, Dandan Wang, Rongfei Yu, Linmin Luo, Weihua Li, Jingsong Cheng, and Yutao Zhang*

Excellent photocatalytic degradation of rhodamine B over Bi_2O_3 supported on Zn-MOF nanocomposites under visible light

https://doi.org/10.1515/gps-2022-8123
received October 05, 2022; accepted January 11, 2023

Abstract: In this article, Bi_2O_3@Zn-MOF hybrid nanomaterials were synthesized by supporting Zn-based metal–organic framework (Zn-MOF) through the hydrothermal method. X-ray diffractometer, Fourier transform infrared, scanning electron microscopy, energy-dispersive X-ray, N_2 physisorption, X-ray photoelectron spectroscopy, and UV-Vis were used to characterize the physical and chemical properties of Bi_2O_3@Zn-MOF nanomaterials. The photocatalytic activity of the as-prepared hybrid has been studied over the degradation of rhodamine B (RhB). A catalytic activity of 97.2% was achieved using Bi_2O_3@Zn-MOF nanocomposite with the loading of 0.18 g Bi_2O_3, after 90 min of exposure to visible light irradiation, and the high photocatalytic performance was mainly associated with the nanorod structures, larger pore size, and broaden visible light absorption region due to the synergistic effect of the constituting materials. Furthermore, the Bi_2O_3@Zn-MOF nanocomposite can be reused three times and the degradation rate of RhB was maintained at 77.9%. Thus, the Bi_2O_3@Zn-MOF nanocomposite can act as a potential photocatalyst for the photodegradation of organic dyes in environmental applications.

Keywords: bismuth oxide, metal–organic framework, photocatalysis, organic pollutants, photodegradation

*** Corresponding author: Qiuyun Zhang,** School of Chemistry and Chemical Engineering, Anshun University, Anshun 561000, Guizhou, China; College Rural Revitalization Research Center of Guizhou, Anshun University, Anshun, 561000, Guizhou, China; Engineering Technology Center of Control and Remediation of Soil Contamination of Guizhou Science and Technology Department, Anshun University, Anshun, 561000, Guizhou, China, e-mail: sci_qyzhang@126.com
*** Corresponding author: Yutao Zhang,** School of Chemistry and Chemical Engineering, Anshun University, Anshun 561000, Guizhou, China; College Rural Revitalization Research Center of Guizhou, Anshun, 561000, Guizhou, China; Engineering Technology Center of Control and Remediation of Soil Contamination of Guizhou Science and Technology Department, Anshun University, Anshun, 561000, Guizhou, China, e-mail: zyt0516@126.com
Dandan Wang, Rongfei Yu, Linmin Luo, Weihua Li, Jingsong Cheng: School of Chemistry and Chemical Engineering, Anshun University, Anshun 561000, Guizhou, China

1 Introduction

Nowadays, with the development of textile industry, water pollution has become a serious environmental issue [1,2]. More than ever, the removal of organic pollutants from wastewater has become a necessity, especially organic synthetic dyes, e.g., rhodamine B (RhB), acridine orange (AO), and methylene blue (MB) [3,4]. According to a research survey, some studies have reported the use of various technologies to remove organic dyes in the wastewater, such as adsorption, biodegradation, ion exchange, and photodegradation [5–7]. Among diverse technologies, photocatalytic reduction is a widely used method by inexhaustible solar energy [8]. Currently, several photocatalysts based on semiconductors (e.g., TiO_2, ZnO, and ZnS) have been widely applied to photocatalysis [9]. Particularly, pure Bi_2O_3 has wide bandgap energy (2.0–3.9 eV) and exhibits significant visible light-responsive photocatalytic performance. Meanwhile, it has the merits of nontoxicity, excellent chemical stability, and abundant earth reserves [10–13]. Nevertheless, pure Bi_2O_3 is still limited, which can be related to its low interfacial area that limits electron transfer, and the easy recombination of electrons and holes [14]. In order to improve the photocatalytic activity of pure Bi_2O_3 photocatalysts, loading Bi_2O_3 into porous nanomaterials is one of the efficient methods.

Recently, metal–organic framework (MOF) has drawn extensive attention due to uniformly structural arrangements, high surface area, tunable pore size, rich functional sites, and excellent adsorption ability [15–17]. Besides, MOF materials have also been exploited as semiconductor-like

photocatalysts, which can be related to the organic ligands of MOF being excited and transferring electrons to the metal center under visible light irradiation [18,19]. Among numerous MOFs, MOF-5 is a relatively highly coordinated Zn-based metal–organic framework (Zn-MOF) with excellent properties, which was considered as a photogenerated charge carrier to enhance the photocatalytic activity [20]. Hence, a feasible approach should be combining Zn-MOF with Bi_2O_3 for photocatalytic research.

Based on the aforementioned considerations, a series of Bi_2O_3@Zn-MOF composites were prepared via the one-pot hydrothermal method, and the photocatalytic performance of the composite was investigated for the degradation of RhB under visible light irradiation condition. The morphology, elemental composition, specific surface area, and structure of the composites were characterized through X-ray diffractometer (XRD), Fourier transform infrared (FTIR), scanning electron microscopy (SEM), energy-dispersive X-ray (EDX), N_2 physisorption, X-ray photoelectron spectroscopy (XPS), UV-Vis, etc. Moreover, the degradation rate of RhB by Bi_2O_3@Zn-MOF composite system under different catalyst dosages and initial RhB concentration was investigated. Importantly, repetitive experiments and photocatalytic degradation of different organic dyes were also carried out. Finally, the possible photocatalytic reaction mechanism on photocatalytic degradation of RhB was analyzed.

2 Materials and methods

2.1 Chemicals

Bismuth trioxide (Bi_2O_3), zinc(II) nitrate hexahydrate ($Zn(NO_3)_2{\cdot}6H_2O$), terephthalic acid (H_2BDC), *N*,*N*-dimethylformamide (DMF), RhB, congo red (CR), AO, neutral red (NR), and MB were purchased from Sigma-Aldrich. All the aforementioned chemicals were of analytical grade and were used as received without further purification. Moreover, deionized water was used in all experiments.

2.2 Synthesis

The Bi_2O_3@Zn-MOF nanocomposites were obtained by the hydrothermal method. In this method, $Zn(NO_3)_2{\cdot}6H_2O$ (0.59 g, 2 mmol) and H_2BDC (0.33 g, 2 mmol) were dissolved in DMF (18 mL), and a certain amount of Bi_2O_3 was added to the above mixture, sonicated for 30 min at room temperature. Subsequently, the solution was stirred for 1 h and then transferred to an autoclave to be heated at 150°C for 6 h. The autoclave was cooled to room temperature, the mixture was centrifuged, and the precipitate was washed with an appropriate amount of DMF for 2 h, followed by washing several times with DMF and water, and dried overnight at 60°C under a vacuum to obtain the Bi_2O_3@Zn-MOF-x nanomaterials, x = 1, 2, and 3, corresponding to the addition of 0.14, 0.18, and 0.22 g Bi_2O_3, and the mole ratio of $Bi_2O_3/Zn(NO_3)_2{\cdot}6H_2O$ was 0.15, 0.195, and 0.235, respectively. For comparison, Zn-MOF was synthesized through the same preparation process without Bi_2O_3.

2.3 Characterization techniques

FTIR spectra were applied to determine the chemical features of the nanocomposites on a PerkinElmer spectrum 100 using KBr pellet technology (4,000–400 cm^{-1}). The XRD studies of the synthesized materials were investigated with D8 ADVANCE (Germany) using CuKĮ (1.5406 Å) radiation. The morphology of the synthesized materials was observed by SEM (Hitachi S4800), and the elemental mapping by EDX was performed on the scanning SEM mode. The surface area and particle sizes of the nanocomposites were studied using N_2 adsorption and desorption isotherms using a Quantachrome Quadrasorb EVO apparatus (Quantachrome Instruments, Boynton Beach, USA). Measurements of XPS were recorded in the Thermo ESCALAB 250XI. The UV-Vis spectra of the synthesized materials were measured by a UV-Vis spectrophotometer (Shimadzu, UV-3600 PLUS, Japan).

2.4 Photodegradation test

The photocatalytic performance of all composites was assessed by RhB degradation. In the photocatalytic process, a certain amount of the nanomaterial was put into 50 mL of RhB solution (40 $mg{\cdot}L^{-1}$). To reach the adsorption–desorption equilibrium, the mixture was stirred in the dark for 0.5 h. Subsequently, the resulting solution was irradiated under visible light with a 300 W xenon lamp for 90 min. After every interval of 30 min, the suspension samples (3–4 mL) were taken from the reaction system and centrifuged to remove the catalyst, and the RhB concentration was determined by a UV-5200PC spectrophotometer (at the characteristic wavelength of 554 nm for RhB). The photodegradation rate of RhB was calculated as follows:

$$\eta = (1 - C/C_0) \times 100\% = (1 - A/A_0) \times 100\%$$

where C_0 is the initial mass concentration of dye solution, A_0 is the corresponding absorbance of dye solution before the reaction, and C and A are the mass concentration and absorbance corresponding to the solution at time t, respectively.

3 Results and discussion

3.1 Characterization

The XRD patterns of synthesized Zn-MOF, Bi_2O_3@Zn-MOF-1, Bi_2O_3@Zn-MOF-2, and Bi_2O_3@Zn-MOF-3 are shown in Figure 1a. The characteristic XRD patterns of Zn-MOF sample (8.8°, 12.0°, 16.8°, 25.4°, 27.8°, 35.4°, and 45.4°) in Figure 1a matched perfectly with those in the previous report [21,22], implying the generation of Zn-MOF. After the induction of Bi_2O_3, some XRD peaks of Zn-MOF-1 disappeared, and the appearance of new peaks of Bi_2O_3@Zn-MOF is also observed at 27.4°, 29.6°, and 33.2°, which are corresponding to the phase of Bi_2O_3 [23], which may be due to the relatively strong interaction between Bi_2O_3 and Zn-MOF. In the case of all composites (Bi_2O_3@Zn-MOF-1, Bi_2O_3@Zn-MOF-2, and Bi_2O_3@Zn-MOF-3), the characteristic diffraction peaks of three composites matched well. In addition, the intensity of the observed characteristic diffraction peaks increased with increasing Bi_2O_3 content. Based on the above analysis, the successful preparation of Bi_2O_3@Zn-MOF composites is clearly demonstrated.

To analyze the functional groups of synthesized Zn-MOF, Bi_2O_3@Zn-MOF-1, Bi_2O_3@Zn-MOF-2, and Bi_2O_3@Zn-MOF-3, FTIR spectroscopy was used (Figure 1b). In Figure 1b, for Zn-MOF, the characteristic peaks between 700 and 1,600 cm^{-1} were related to C═O, C–O, and C═C stretching vibration in carboxylic acid [24]. In comparison with Zn-MOF, similar peaks also appeared in the spectra of all Bi_2O_3@Zn-MOF composites, which proves that the structure of Zn-MOF was not changed after the introduction of Bi_2O_3 into the Zn-MOF. In particular, the appeared band at 519 cm^{-1} in Bi_2O_3@Zn-MOF composites was attributed to Bi–O of Bi_2O_3 [25], which indicates that the successful impregnation of Bi_2O_3 is on the framework of the Zn-MOF.

The structure and morphology of the as-prepared Zn-MOF and Bi_2O_3@Zn-MOF with different additions of Bi_2O_3 were observed by SEM, as shown in Figure 2. In Figure 2a, the Zn-MOF sample is irregular nanosheets with thickness in the range of 30–50 nm. When the wrapping of Bi_2O_3, Bi_2O_3@Zn-MOF-1 sample is composed of irregular nanosheets and rod-shaped structure (Figure 2b). With increasing Bi_2O_3 content, sample Bi_2O_3@Zn-MOF-2 (Figure 2c and e) exhibits quite different morphologies compared with Zn-MOF and Bi_2O_3@Zn-MOF-1 samples. It has a typical branched nanorod, and the existence of abundant pores may result in better adsorption of dye molecules and improves the catalytic material photocatalytic activity. For sample Bi_2O_3@Zn-MOF-3 (Figure 2d), the agglomeration of rod-shaped particles and large irregular lumpy structure by the shrinkage of the Bi_2O_3@Zn-MOF-3 composite was clear. This was possible because of the effect of the formation of Zn-MOF framework by the addition of excess Bi_2O_3. Additionally, the EDX elemental

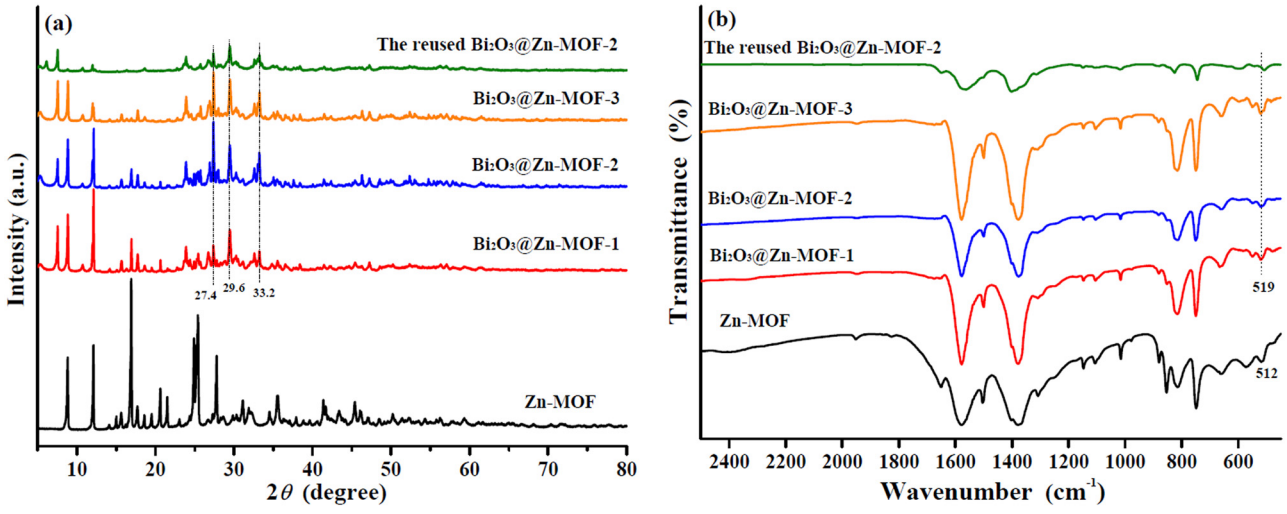

Figure 1: XRD (a) and FTIR (b) spectra of Zn-MOF, Bi_2O_3@Zn-MOF-1, Bi_2O_3@Zn-MOF-2, Bi_2O_3@Zn-MOF-3, and the recovered Bi_2O_3@Zn-MOF-2 sample.

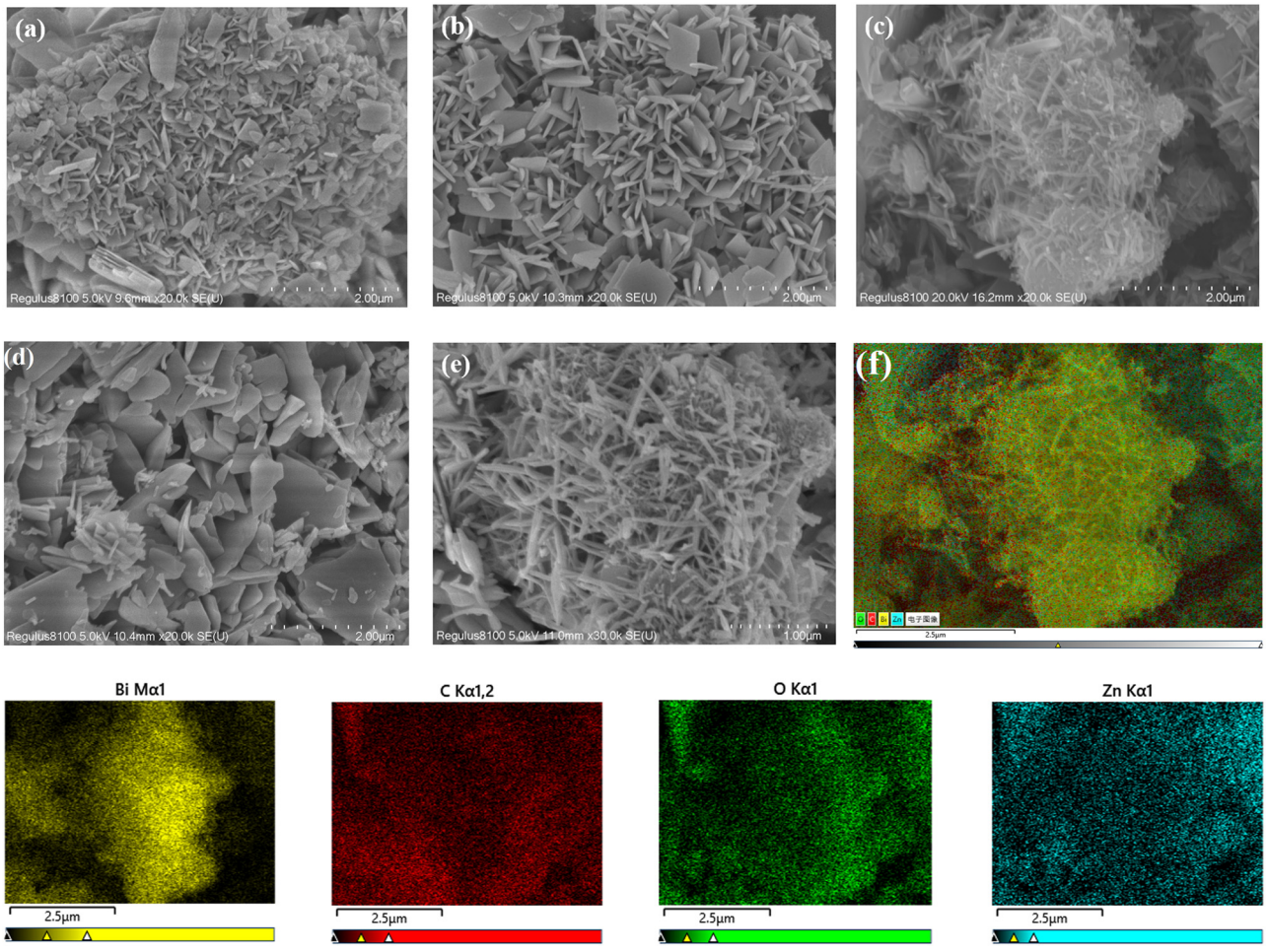

Figure 2: SEM images of Zn-MOF (a), Bi_2O_3@Zn-MOF-1 (b), Bi_2O_3@Zn-MOF-2 (c and e), and Bi_2O_3@Zn-MOF-3 (d), and (f) the EDX analysis of Bi_2O_3@Zn-MOF-2 sample and the related elemental mapping photographs of Bi, C, O, and Zn.

mappings of Bi_2O_3@Zn-MOF-2 were further analyzed. As can be seen from Figure 2f, Bi, C, O, and Zn elements are present in the Bi_2O_3@Zn-MOF-2 composite. Besides, the Bi and O elements were uniformly distributed over the Bi_2O_3@Zn-MOF-2 composite, indicating that Bi_2O_3 adheres to the surface of the Zn-MOF. The EDX analysis results are consistent with results of the XRD and FTIR analysis.

Figure 3a shows the N_2 adsorption–desorption isotherm curves of Zn-MOF and Bi_2O_3@Zn-MOF-2. All the N_2 adsorption–desorption curves show type IV adsorption, and their hysteresis loops reveal H3 type. Moreover, it can be known from Figure 3b that the pore sizes of Zn-MOF and Bi_2O_3@Zn-MOF-2 are mainly distributed in the range of 4–8 nm, which are characteristics of mesoporous materials. According to previous studies, the surface area and pore volume of pure Bi_2O_3 are 4.3 $m^2 \cdot g^{-1}$ and 0.018 $cm^3 \cdot g^{-1}$, respectively, indicating that pure Bi_2O_3 exhibits a low surface area and pore volume [26]. Interestingly, from Table 1, the incorporation of Bi_2O_3 slightly decreased the surface area and increased the average pore size of Zn-MOF, and this could be explained by partial obstruction of mesoporous materials by Bi_2O_3 particles. Furthermore, it should be noted that the larger size of the Bi_2O_3@Zn-MOF-2 catalyst pore structure will provide abundant surface adsorption and active sites, and further resulting in enhancement of the photocatalytic activity.

The elemental compositions and the chemical states of Bi_2O_3@Zn-MOF-2 were further evaluated using XPS, and the obtained results are given in Figure 4. In Figure 4a, the XPS full spectrum clearly shows that C, Zn, and Bi elements exist in Bi_2O_3@Zn-MOF-2 composites. The XPS spectrum of C 1s (Figure 4b) presents two peaks at 284.6 and 288.8 eV that can be assigned to the C═C and C═O bonds, respectively [27]. The Zn 2p XPS spectra located at 1,022.8 and 1,045.9 eV are related to the Zn $2p_{3/2}$ and Zn $2p_{1/2}$, respectively (Figure 4c), indicating that Zn is +2 valent [28]. Finally, for the Bi 4f spectra shown in Figure 4d, the peaks at 159.5 and 164.8 eV can be matched to Bi $4f_{7/2}$ and Bi $4f_{5/2}$, revealing

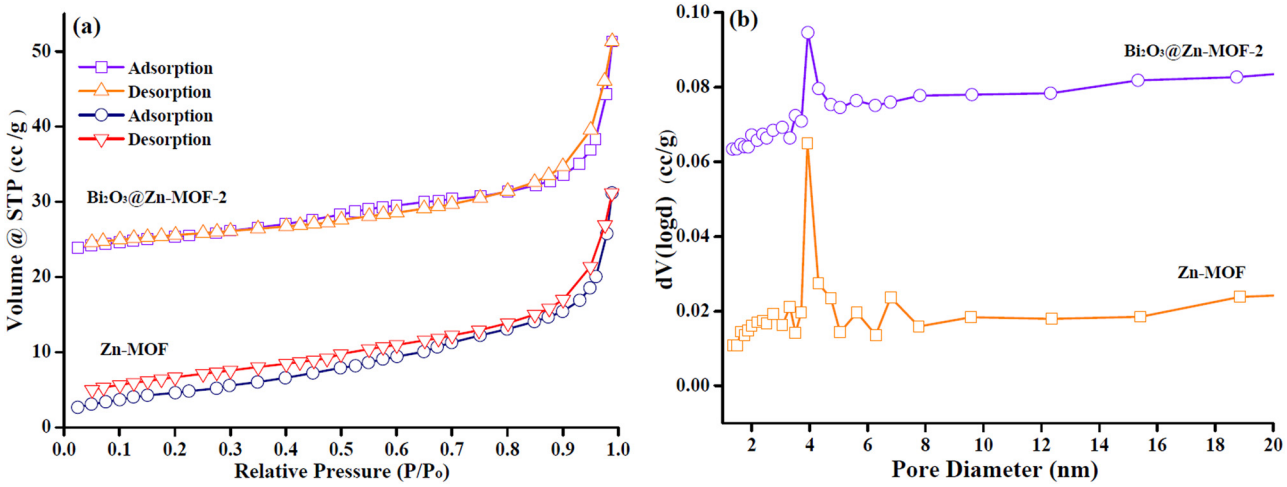

Figure 3: N_2 adsorption–desorption isotherms (a) and pore size distribution (b) of Zn-MOF and Bi_2O_3@Zn-MOF-2.

Table 1: Textural parameters of Zn-MOF and Bi_2O_3@Zn-MOF-2

Entry	Sample type	Surface area ($m^2 \cdot g^{-1}$)	Average pore size (nm)	Pore volume ($cm^3 \cdot g^{-1}$)
1	Zn-MOF	17.51	11.02	0.048
2	Bi_2O_3@Zn-MOF-2	13.21	13.74	0.045

the Bi^{3+} in Bi_2O_3@Zn-MOF-2 [29]. XPS analysis also proved that the successful synthesis of Bi_2O_3 on the Zn-MOF by the hydrothermal method.

The UV-Vis diffuse reflection spectroscopy (DRS) was also measured to examine the light absorption performances of Bi_2O_3@Zn-MOF-2 composite (Figure 5). As shown in Figure 5, the Bi_2O_3@Zn-MOF-2 composite displays the light absorption peak ranging between 300 and 460 nm. According to the previous articles, the Zn-MOF sample showed the absorption of light below 400 nm, and the absorption edge was about 379.7 nm [30]. After the introduction of Bi_2O_3, the Bi_2O_3@Zn-MOF-2 sample exhibited an absorption edge around 453 nm, and the light absorption was extended further to the visible region. The shift suggests that the existence of the synergistic effect between Bi_2O_3 and Zn-MOF in the Bi_2O_3@Zn-MOF-2 composite can enhance the absorption of visible light, resulting in the improvement of the photodegradation ability.

3.2 Photocatalytic activity of different photocatalysts

Figure 6a shows the RhB degradation over different photocatalysts. From Figure 6a, in the absence of catalyst, the RhB has no obvious degradation for 90 min, representing that the RhB is a stable and difficult to degrade organic dye. Both Zn-MOF and Bi_2O_3 samples were not effective in the degradation of RhB. However, it was found that after introduction of Bi_2O_3, the RhB degradation further obviously increased. Additionally, Bi_2O_3@Zn-MOF-2 showed higher photocatalytic activity than Bi_2O_3@Zn-MOF-1 and Bi_2O_3@Zn-MOF-3. In contrast, the Bi_2O_3@Zn-MOF-2 under light-free condition only showed some adsorption activity. Figure 6b shows the proposed pseudo-first-order kinetics for the photocatalytic degradation of RhB by Bi_2O_3@Zn-MOF with the addition of different mass ratios of Bi_2O_3, the degradation rate constants of Bi_2O_3@Zn-MOF-2 are 1.67 and 1.06 times higher than that of Bi_2O_3@Zn-MOF-1 and Bi_2O_3@Zn-MOF-3, it may be due to the Bi_2O_3@Zn-MOF-2 can provide a large pore size and abundant transport pores, and increasing the visible light irradiation. Thus, the Bi_2O_3@Zn-MOF-2 is chosen as the optimal photocatalyst.

3.3 Effect of the catalyst amount and RhB concentration

To investigate the effect of the Bi_2O_3@Zn-MOF-2 catalyst amount on the photocatalytic degradation of RhB,

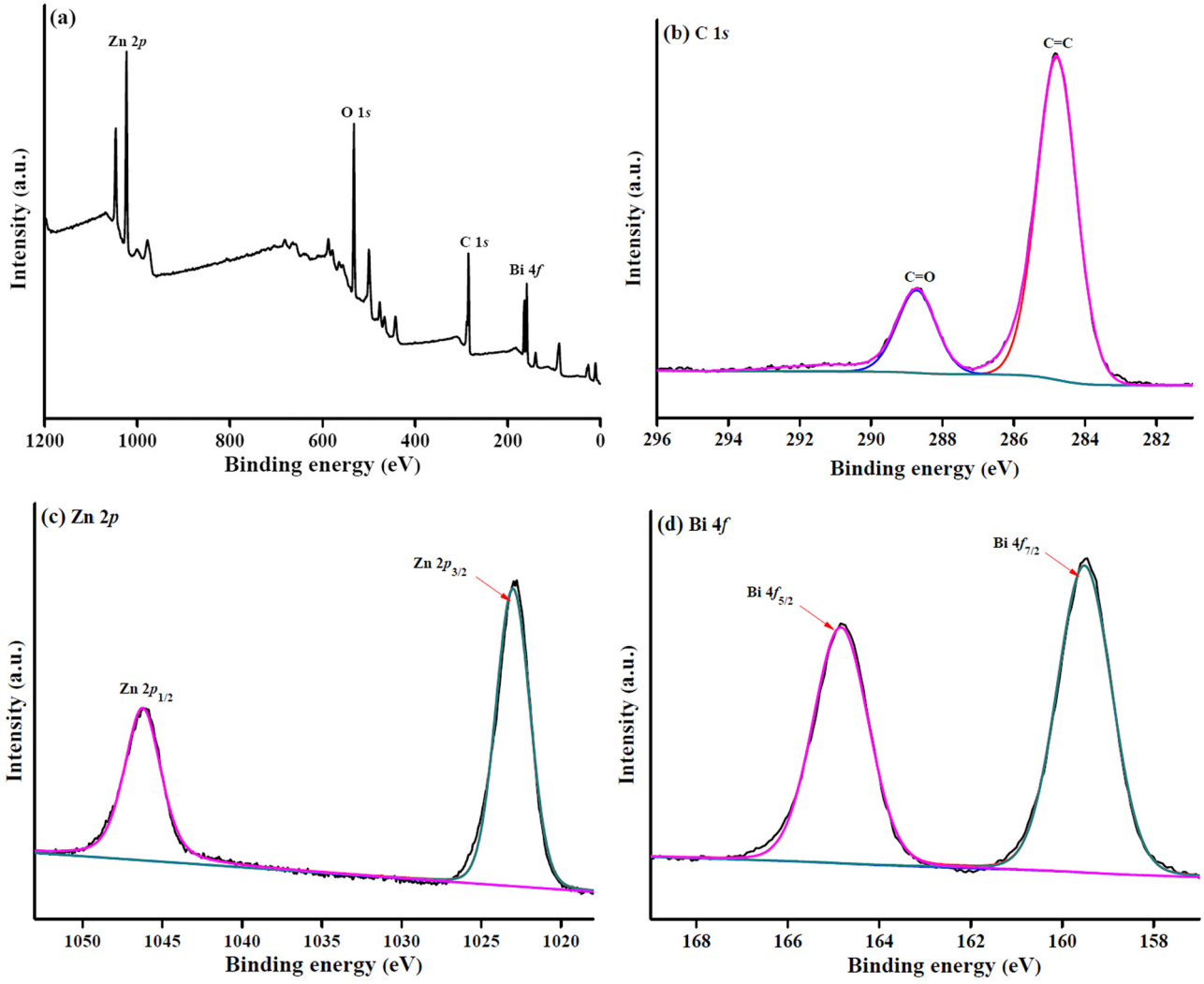

Figure 4: XPS full spectrum (a), C 1s spectrum (b), Zn 2p spectrum (c), and Bi 4f spectrum (d) of the Bi_2O_3@Zn-MOF-2 composite.

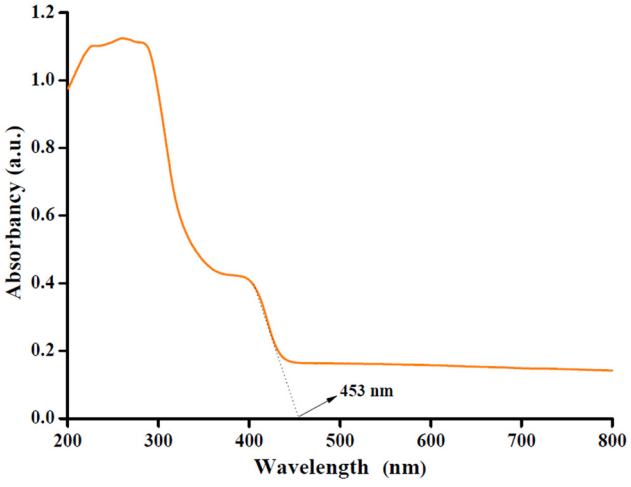

Figure 5: UV-Vis light DRS of Bi_2O_3@Zn-MOF-2 composite.

different amounts of catalyst (0.6, 1.0, and 1.4 g·L^{-1}) were added to the photocatalytic system and the degradation profiles are depicted in Figure 7a. With the increase in catalyst amount, the degradation rate of RhB was also increased. It can see that the increase in catalyst amount may increase the number of active sites and the contact probability between dye molecules and Bi_2O_3@Zn-MOF-2. However, when the amount of Bi_2O_3@Zn-MOF-2 increased to a certain level, the degradation rate was also slightly increased. This phenomenon may be attributed to the agglomeration of the catalyst leading to decrease in the radiation absorption, and as a result, the degradation rate was not significant change [31]. Therefore, the amount of catalyst was 1.0 g·L^{-1}.

The influence of initial RhB concentration on photocatalytic degradation activity of the Bi_2O_3@Zn-MOF-2 was

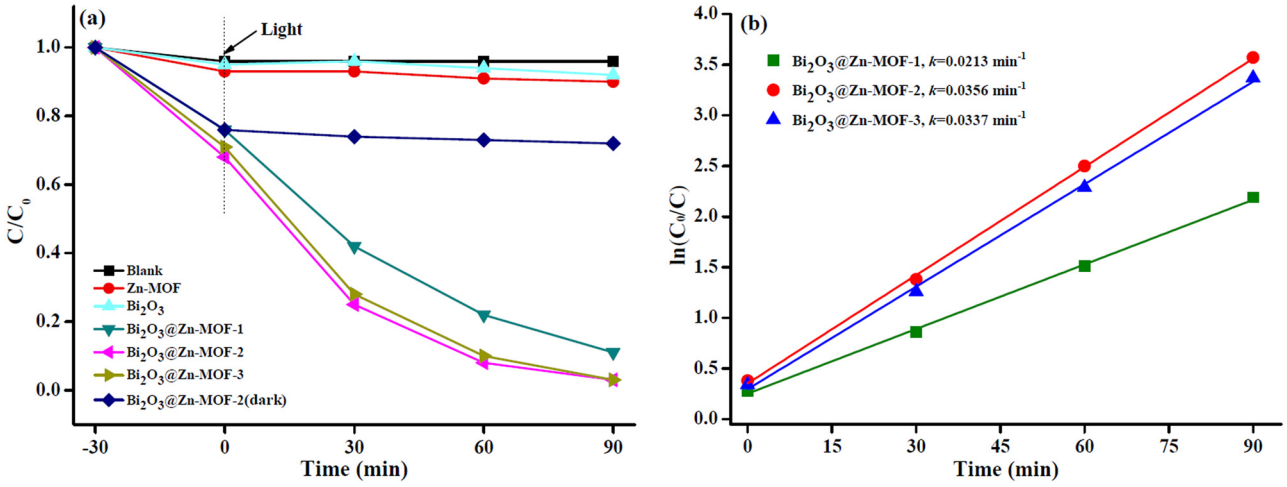

Figure 6: (a) Photocatalytic degradation of RhB with different catalysts under visible light irradiation. (b) Pseudo-first-order kinetics plots of photocatalytic degradation of RhB with different catalysts.

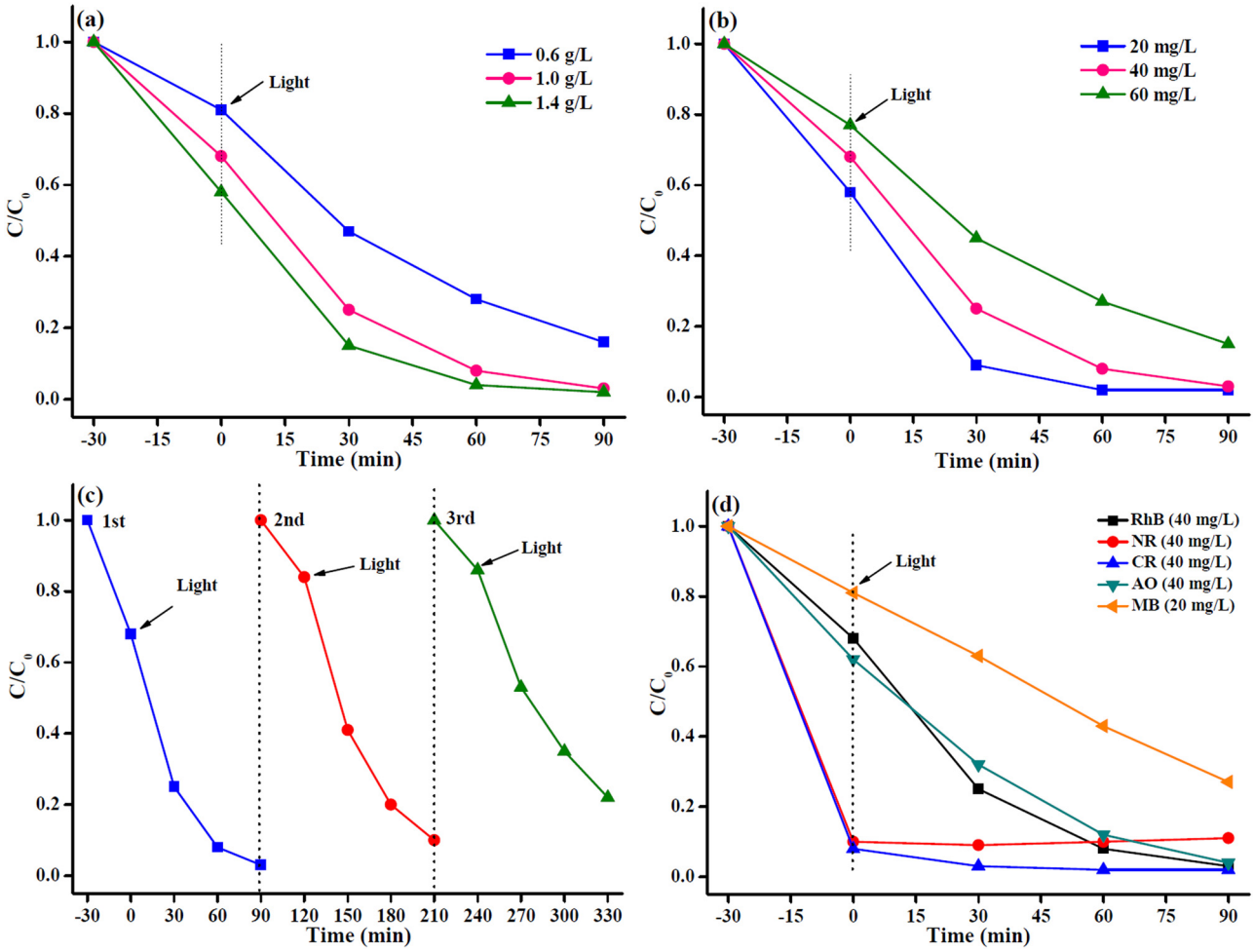

Figure 7: (a) Photocatalytic degradation of RhB with various dosages of Bi_2O_3@Zn-MOF-2 catalyst. (b) Photocatalytic degradation of RhB with different concentrations using Bi_2O_3@Zn-MOF-2 catalyst. (c) Cyclic stability of Bi_2O_3@Zn-MOF-2 catalyst after three cycles. (d) Photocatalytic degradation of various organic dyes using Bi_2O_3@Zn-MOF-2 catalyst.

studied (Figure 7b). The degradation rate gradually decreased as the RhB concentration increased from 20 to 60 mg·L^{-1}. When the concentration of RhB is increased, it is probably related to more molecules to present around photocatalytic active sites, and thus, the light transmission capacity of the system decreases, leading to reduce the electron and hole pairs [32], and resulting in decrease in the degradation rate.

3.4 Stability test

To evaluate the stability of the Bi_2O_3@Zn-MOF-2 catalyst for its repetitive use, the repeated RhB degradation rate was investigated for three cycles. In each cycle experiment, the Bi_2O_3@Zn-MOF-2 catalyst can be directly separated via centrifugation, and then washed, dried, and applied in the next experiment, and the experiment results are indicated in Figure 7c. Indeed, the photocatalytic degradation rate of RhB decreased from 97.2% to 77.9% after three cycles, which is probably due to the partial loss of the Bi_2O_3@Zn-MOF-2 catalyst throughout the cycling tests. Moreover, FTIR and XRD patterns of Bi_2O_3@Zn-MOF-2 catalyst after three recycling experiments were investigated and compared to the fresh catalyst. As shown in Figure 1, the results reveal that no significant changes occurred in the characteristic diffraction peaks, but the strength of the peaks weakened after three cycles. Furthermore, all these confirm that the Bi_2O_3@Zn-MOF-2 catalyst is a better stability photocatalyst.

3.5 Photocatalytic degradation of different organic dyes

The degradation rate of the Bi_2O_3@Zn-MOF-2 catalyst for five organic dyes under visible light irradiation within 90 min was studied, and the results are shown in Figure 7d. For NR and CR degradation, the adsorption saturation was reached at 30 min of lightless reaction with the presence of the catalyst, resulting in good adsorption of those two dyes. Moreover, clearly seen, the photocatalytic performances of the Bi_2O_3@Zn-MOF-2 catalyst were 97.2%, 96.1%, and 73.1% for RhB (40 mg·L^{-1}), AO (40 mg·L^{-1}), and MB (20 mg·L^{-1}) degradation under visible light irradiation, respectively. It follows that the as-synthesized Bi_2O_3@Zn-MOF-2 catalyst can effectively degrade other organic dyes, and it can also be an excellent candidate for application in industrial wastewater treatment processes.

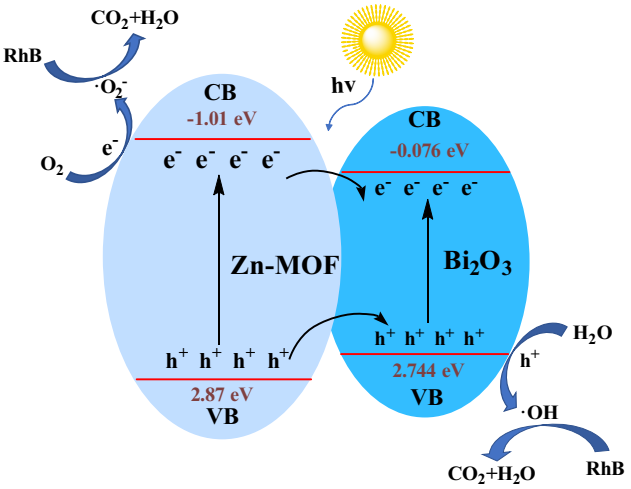

Figure 8: Possible photocatalytic mechanisms of RhB solution using Bi_2O_3@Zn-MOF-2 catalyst.

3.6 Possible photocatalytic mechanisms

Possible photocatalytic mechanism for degradation of RhB solution with Bi_2O_3@Zn-MOF-2 composite photocatalyst is illustrated in Figure 8. Under visible light irradiation, electrons (e^-) and holes (h^+) can be generated from Bi_2O_3@Zn-MOF-2. According to the literature, the conduction band (CB) potential (E_{CB}) and valence band (VB) potential (E_{VB}) of Bi_2O_3 are −0.076 and 2.744 eV, respectively [33]. The E_{CB} and E_{VB} of Zn-MOF are −1.01 and 2.87 eV, respectively [34]. Then, h^+ transfers from the VB of Zn-MOF to the VB of Bi_2O_3, and e^- transfers from the CB of Zn-MOF to the CB of Bi_2O_3, resulting in efficient separation of e^-–h^+ pairs in Bi_2O_3@Zn-MOF-2 composite. Subsequently, the VB edge of Bi_2O_3 and Zn-MOF has a more positive VB potential than oxidation potential energy of $H_2O/^{\cdot}OH$ (2.7 eV), and the partial h^+ can participate in the generation of $^{\cdot}OH$ from H_2O. Also, the position of the Zn-MOF conduction band is higher than the oxidation potential energy of $O_2/^{\cdot}O_2^-$ (−0.3 eV), and the e^- of Zn-MOF can reduce O_2 into $\cdot O_2^-$. The generated active species can decompose the organic dyes into CO_2 and H_2O, and finally achieve photocatalytic degradation. Based on this, in our system, the synergistic effect between Bi_2O_3 and Zn-MOF of Bi_2O_3@Zn-MOF-2 composite would achieve highly efficient organic dye photodegradation.

4 Conclusion

This study aimed to successfully synthesize Bi_2O_3 supported on Zn-MOF nanocomposites (Bi_2O_3@Zn-MOF) with

different Bi_2O_3 concentrations for the photocatalytic degradation of RhB under visible light irradiation. Among them, Bi_2O_3@Zn-MOF-2 has the highest photodegradation activity compared to Bi_2O_3, Zn-MOF, and Bi_2O_3@Zn-MOF-1 and Bi_2O_3@Zn-MOF-3, which is related to the relatively larger specific surface area and pore size, the nanorods morphology, the synergistic effect the constituting materials lead to expand visible light absorption range. After 90 min of photocatalytic reaction, the degradation rate of RhB for Bi_2O_3@Zn-MOF-2 nanocomposite was estimated to be 97.2%. After three cycles, the degradation rate of RhB is still above 77.9%, and it has good reusability. Meanwhile, tests for the photodegradation of CR, AO, and MB also revealed that the Bi_2O_3@Zn-MOF-2 nanocomposite was an efficient photocatalyst. Overall, the obtained Bi_2O_3@Zn-MOF nanocomposites might be considered for application in the field of wastewater treatment.

Funding information: This work was financially supported by the National Natural Science Foundation of China (22262001), the 2018 Thousand Level Innovative Talents Training Program of Guizhou Province, the Anshun Science and Technology Planning Project ([2021]1), the Guizhou Science and Technology Foundation ([2020]1Y054), the 2022 Innovative Entrepreneurship Training Program for Undergraduates of the Guizhou Education Department (202210667017), and the Student Research Training of Anshun University (asxysrt202202).

Author contributions: Qiuyun Zhang: writing – original draft, writing – review and editing, methodology, formal analysis, project administration; Dandan Wang: methodology, formal analysis; Rongfei Yu: methodology, formal analysis; Linmin Luo: methodology, formal analysis; Weihua Li: visualization; Jingsong Cheng: visualization; Yutao Zhang: project administration.

Conflict of interest: The authors state no conflict of interest.

Data availability statement: All data generated or analyzed during this study are included in this published article.

References

[1] Hou JW, Yang HD, He BY, Ma JG, Lu Y, Wang QY. High photocatalytic performance of hydrogen evolution and dye degradation enabled by CeO_2 modified TiO_2 nanotube arrays. Fuel. 2022;310:122364.
[2] Yang GH, Zhang DQ, Zhu G, Zhou TR, Song MT, Qu LL, et al. A Sm-MOF/GO nanocomposite membrane for efficient organic dye removal from wastewater. RSC Adv. 2020;10:8540–7.
[3] Alshammari AS, Bagabas A, Alarifi N, Altamimi R. Effect of the nature of metal nanoparticles on the photocatalytic degradation of rhodamine B. Top Catal. 2019;62:786–94.
[4] Mahmoodi NM. Surface modification of magnetic nanoparticle and dye removal from ternary systems. J Ind Eng Chem. 2015;27:251–9.
[5] Khan M, Ali SW, Shahadat M, Sagadevan S. Applications of polyaniline-impregnated silica gel-based nanocomposites in wastewater treatment as an efficient adsorbent of some important organic dyes. Green Process Synth. 2022;11:617–30.
[6] Wang TT, Yang YT, Lim SC, Chiang CL, Lim JS, Lin YC, et al. Hydrogenation engineering of bimetallic Ag-Cu-modified-titania photocatalysts for production of hydrogen. Catal Today. 2022;388–389:79–86.
[7] Mahmoodi NM, Mokhtari-Shourijeh Z. Preparation of PVA-chitosan blend nanofiber and its dye removal ability from colored wastewater. Fibers Polym. 2015;16:1861–9.
[8] Khan F, Khan MS, Kamal S, Arshad M, Ahmad SI, Nami SAA. Recent advances in graphene oxide and reduced graphene oxide based nanocomposites for the photodegradation of dyes. J Mater Chem C. 2020;8:15940–55.
[9] Lian P, Qin AM, Liao L, Zhang KY. Progress on the nanoscale spherical TiO_2 photocatalysts: Mechanisms, synthesis and degradation applications. Nano Sel. 2021;2:447–67.
[10] Natarajan K, Bajaj HC, Tayade RJ. Photocatalytic efficiency of bismuth oxyhalide (Br, Cl and I) nanoplates for RhB dye degradation under LED irradiation. J Ind Eng Chem. 2016;34:146–56.
[11] Devika S, Tayade RJ. Low temperature energy-efficient synthesis methods for bismuth-based nanostructured photocatalysts for environmental remediation application: A review. Chemosphere. 2022;304:135300.
[12] Limpachanangkul P, Liu LC, Hunsom M, Piumsomboon P, Chalermsinsuwan B. Application of Bi_2O_3/TiO_2 heterostructures on glycerol photocatalytic oxidation to chemicals. Energy Rep. 2022;8:1076–83.
[13] Sharma A, Sharma S, Mphahlele-Makgwane MM, Mittal A, Kumari K, Kumar N. Polyaniline modified Cu^{2+}-Bi_2O_3 nanoparticles: Preparation and photocatalytic activity for Rhodamine B degradation. J Mol Structure. 2023;1271:134110.
[14] Jiang HY, Liu JJ, Cheng K, Sun WB, Lin J. Enhanced visible light photocatalysis of Bi_2O_3 upon fluorination. J Phys Chem C. 2013;117:20029–36.
[15] Zhang QY, Zhang YT, Cheng JS, Li H, Ma PH. An overview of metal-organic frameworks-based acid/base catalysts for biofuel synthesis. Curr Org Chem. 2020;24:1876–91.
[16] Yadav S, Dixit R, Sharma S, Dutta S, Solanki K, Sharma RK. Magnetic metal-organic framework composites: structurally advanced catalytic materials for organic transformations. Mater Adv. 2021;2:2153–87.
[17] Zhang QY, Wang JL, Zhang SY, Ma J, Cheng JS, Zhang YT. Zr-based metal-organic frameworks for green biodiesel synthesis: A minireview. Bioengineering. 2022;9:700.
[18] Xiao JD, Jiang HL. Metal-organic frameworks for photocatalysis and photothermal catalysis. Acc Chem Res. 2019;52:356–66.

[19] Jiang W, Li Z, Liu CB, Wang DD, Yan GS, Liu B, et al. Enhanced visible-light-induced photocatalytic degradation of tetracycline using BiOI/MIL-125(Ti) composite photocatalyst. J Alloy Compd. 2021;854:157166.
[20] Yang HM, Liu X, Song XL, Yang TL, Liang ZH, Fan CM. In situ electrochemical synthesis of MOF-5 and its application in improving photocatalytic activity of BiOBr. Trans Nonferrous Met Soc China. 2015;25:3987–94.
[21] Phan NTS, Le KKA, Phan TD. MOF-5 as an efficient heterogeneous catalyst for Friedel-Crafts alkylation reactions. Appl Catal A-General. 2010;382:246–53.
[22] Yang M, Baia QH. Flower-like hierarchical Ni-Zn-MOF microspheres: Efficient adsorbents for dye removal. Colloids Surf A. 2019;582:123795.
[23] Rahman NJA, Ramli A, Jumbri K, Uemura Y. Biodiesel production from *N. oculata* microalgae lipid in the presence of Bi_2O_3/ZrO_2 catalysts. Waste Biomass Valoriz. 2020;11:553–64.
[24] Celebi N, Aydin MY, Soysal F, Yıldız N, Salimi K. Core/shell PDA@UiO-66 metal-organic framework nanoparticles for efficient visible-light photodegradation of organic dyes. ACS Appl Nano Mater. 2020;3:11543–54.
[25] Yang Q, Wei SQ, Zhang LM, Yang R. Ultrasound-assisted synthesis of $BiVO_4$/C-dots/g-C_3N_4 Z-scheme heterojunction photocatalysts for degradation of minocycline hydrochloride and Rhodamine B: optimization and mechanism investigation. N J Chem. 2020;44:17641–53.
[26] Song Q, Li L, Luo HX, Liu Y, Yang CL. Hierarchical nanoflower-ring structure $Bi_2O_3/(BiO)_2CO_3$ composite for photocatalytic degradation of rhodamine B. Chin J Inorg Chem. 2017;33:1161–71.
[27] Ahmad M, Chen S, Ye F, Quan X, Afzal S, Yu HT, et al. Efficient photo-Fenton activity in mesoporous MIL-100(Fe) decorated with ZnO nanosphere for pollutants degradation. Appl Catal B: Environ. 2019;245:428–38.
[28] Xu J, Wang XT, Fan CC, Qiao J. Effect of Pd-modification on photocatalytic H_2 evolution over $Cd_{0.8}Zn_{0.2}S/SiO_2$ from glycerol solution. J Fuel Chem Technol. 2013;41:323–7.
[29] Lu MJ, Yang Z, Zhao WF, Li Y. Study on photocatalytic activities of Bi_2WO_6 coupled with wide band-gap semiconductor titanium oxide under visible light irradiation. J Funct Mater. 2018;49:7093–8.
[30] Yang L, Wang Q, Deng YJ, Wang XY, Ren HE, Yi ZY, et al. Effect of metal exchange on the light-absorbing and band-gap properties of nanoporous Zn-Cu based MOFs. Chin J Inorg Chem. 2018;34:1199–208.
[31] Mirzaeifard Z, Shariatinia Z, Jourshabani M, Darvishi SMR. ZnO photocatalyst revisited: Effective photocatalytic degradation of emerging contaminants using S-doped ZnO nanoparticles under visible light radiation. Ind & Eng Chem Res. 2020;59:15894–911.
[32] Li F, Qin SN, Jia S, Wang GY. Pyrolytic synthesis of organosilane-functionalized carbon nanoparticles for enhanced photocatalytic degradation of methylene blue under visible light irradiation. Luminescence. 2021;36:711–20.
[33] Chen QG, Gu FF, Cheng XF, Jin XF. Bi_2O_3-ZnO composite materials: preparation and performance. J Funct Mater. 2017;48:155–9.
[34] Yao TT, Tan YW, Zhou Y, Chen YB, Xiang MH. Preparation of core-shell MOF-5/Bi_2WO_6 composite for the enhanced photocatalytic degradation of pollutants. J Solid State Chem. 2022;308:122882.